Elastohydrodynamic Lift at a Soft Wall

Heather S. Davies,[1] Delphine Débarre,[1] Nouha El Amri,[1] Claude Verdier,[1] Ralf P. Richter,[2,3,*] and Lionel Bureau[1,†]
[1]*Université Grenoble Alpes, CNRS, LIPhy, 38000 Grenoble, France*
[2]*School of Biomedical Sciences, Faculty of Biological Sciences, School of Physics and Astronomy, Faculty of Mathematics and Physical Sciences, Astbury Centre for Structural Molecular Biology, University of Leeds, Leeds LS2 9JT, United Kingdom*
[3]*CIC biomaGUNE, Paseo Miramon 182, 20014 San Sebastian, Spain*

(Received 30 November 2017; revised manuscript received 2 March 2018; published 9 May 2018)

We study experimentally the motion of nondeformable microbeads in a linear shear flow close to a wall bearing a thin and soft polymer layer. Combining microfluidics and 3D optical tracking, we demonstrate that the steady-state bead-to-surface distance increases with the flow strength. Moreover, such lift is shown to result from flow-induced deformations of the layer, in quantitative agreement with theoretical predictions from elastohydrodynamics. This study thus provides the first experimental evidence of "soft lubrication" at play at small scale, in a system relevant, for example, to the physics of blood microcirculation.

DOI: 10.1103/PhysRevLett.120.198001

Elastohydrodynamics (EHD) is a key concept in soft matter physics [1–3]. The coupling between flow-induced pressure fields and elasticity of immersed objects is at the heart of topics ranging from the rheology of soft colloids [4] to microfluidic particle sorting [5] and contact-free mechanical probe techniques [6]. EHD is also central to biophysical problems, such as swimming of microorganisms [7], lubrication in synovial joints, and blood microcirculation [8]. In the latter context, EHD governs the radial migration of circulating blood cells, which underlies vascular processes, such as margination [5,9,10]: leukocytes and platelets flow preferentially close to the vessel walls, while softer red blood cells (RBCs) migrate away from them. This gives rise to a cell-free layer, a μm-thick region forming near the vascular walls and depleted of RBCs [11]. This has been characterized *in vitro*, through flow experiments studying how RBCs [12] or model vesicles [13] are repelled by a surface. The classical interpretation for the formation of the cell-free layer is that RBCs flowing near a surface deform under the fluid shear stress and experience a noninertial lift force that pushes them away from the wall [14]. Reflecting this, most *in vitro* studies, as well as numerical [15] and theoretical [16] works, consider interactions between a rigid surface and deformable cells, which adopt an asymmetric shape under flow. Such an asymmetry of the flowing objects is pinpointed as the origin of the lift force arising at the low Reynolds numbers typically encountered in microcirculation. *In vivo*, however, blood flow takes place in compliant vessels. In particular, the endothelium (the luminal side of blood vessels) is lined by a glycocalyx, a thin (100–1000 nm) and soft (elastic modulus of 10–100 Pa) layer of polysaccharides bound to the walls and directly exposed to blood flow [17]. While the importance of the glycocalyx on blood microrheology is recognized [17–19], its quantitative influence on EHD interactions largely remains to be established. More generally, the question of how a thin deformable layer can contribute to "soft lubrication" and induce lift forces has been addressed theoretically [20–23] but has received limited attention from the experimental standpoint, with a single study investigating at the macroscopic scale how EHD affects the sliding dynamics of cylinders near a soft wall [24]. In this Letter, we report the investigation of the lift experienced by rigid spherical particles flowing in the vicinity of a surface bearing a polymer brush that mimics the glycocalyx. Using microfluidics and three-dimensional (3D) tracking, we provide the first direct evidence that, under conditions of flow strengths and object sizes relevant to blood circulation, a thin deformable polymer brush gives rise to a sizeable lift on circulating beads, which can be quantitatively described by soft lubrication theory.

Experiments were performed at room temperature using a parallel-plate flow chamber (Glycotech, USA) composed of a spacer defining a straight channel [Fig. 1(a)] of rectangular cross section (height $H = 0.250$ mm, width $W = 2.5$ mm, length $L = 20$ mm), sandwiched between an upper deck with fluid inlet and outlet and a bottom surface consisting of a glass coverslip functionalized with a brush of hyaluronan [HA, the major component of the glycocalyx, see Fig. 1(a) and details below]. The inlet reservoir contained spherical polystyrene beads of radius $R = 12.5$ μm (Kisker Biotech, Germany) suspended in aqueous buffer (10 mM HEPES, *p*H 7.4, 150 mM NaCl, 2 mM $CaCl_2$, viscosity $\eta \simeq 10^{-3}$ Pa s, and density $\rho \simeq 1000$ kg m^{-3}), while the outlet was connected to a syringe pump (KDS Legato 110) imposing flow rates in the range $Q = 1$–200 μL min^{-1}. Beads were pumped into the channel and left to sediment

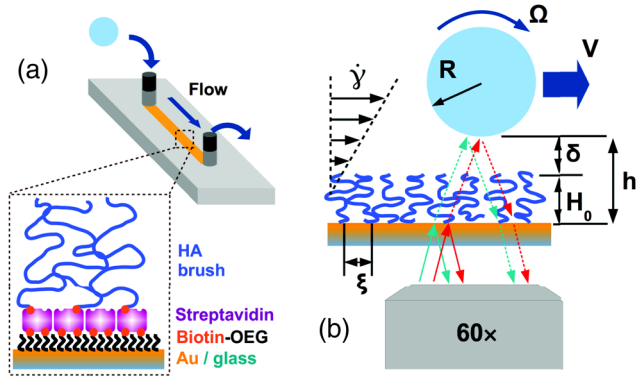

FIG. 1. (a) Flow chamber with bottom surface functionalized with a HA brush via biotin-streptavidin binding. (b) Bead traveling in a shear flow of velocity gradient $\dot{\gamma}$. Dual color RICM is used to monitor its distance h from the substrate and its translation velocity V.

under quiescent conditions onto the bottom surface of the chamber, after which their motion under imposed flow rate was monitored optically. Here, 3D tracking was performed by reflection interference contrast microscopy (RICM) using a setup allowing for simultaneous imaging at two wavelengths ($\lambda_1 = 532$ nm, $\lambda_2 = 635$ nm, see Supplemental Material [25] and Refs. [26,27] for details). Under flow, the fringe patterns due to interference between the light reflected from the substrate and the surface of the beads were recorded [Figs. 2(a) and 2(b)] on a camera (ORCA-Flash4.0 Hamamatsu) at rates of up to 200 frames per second. Bead trajectories were analyzed offline, using home-written Labview routines, in order to compute for

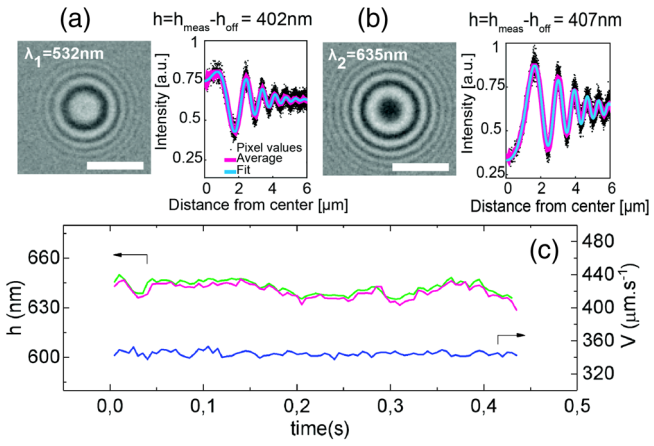

FIG. 2. (a) Left: interference patterns at $\lambda_1 = 532$ nm (scale bar 5 μm). Right: radial intensity profile (black dots) extracted from image, azimuthally averaged (magenta line), and fitted with an optical model (cyan line) to determine h_{meas}, from which we compute $h = h_{\mathrm{meas}} - h_{\mathrm{off}}$, with h_{off} the offset due to the contribution of the gold and streptavidin layers (measured independently, see Supplemental Material [25]). (b) Same as (a) at $\lambda_2 = 635$ nm. (c) Time series for h (green: λ_1, magenta: λ_2) and V (blue), for a bead flowing close to the HA brush.

each Q: (i) the steady-state vertical distance h between the substrate and the beads and (ii) the beads' translation velocity V [Figs. 1(b) and 2(c)]. The absolute value of h was determined unambiguously up to $\sim$1.2 μm owing to the two-color RICM scheme used [27], with an accuracy of $\sim$10 nm. The in-plane displacements of the beads, from which V was computed, were determined by image correlation with an accuracy of $\sim$50 nm.

The surface of the coverslip exposed to the flow was functionalized with a layer of HA, as described in [28,29]. A Ti/Au layer (respectively, 0.5 and 5 nm in thickness) was evaporated onto the glass surface. A monolayer of end-biotinylated oligo(ethyleneglycol) thiols (bOEG-SH) was grafted onto the gold film. A dense layer of streptavidin was bound to the exposed biotin moieties and further functionalized by incubation with end-biotinylated HA [Fig. 1(a)]. Such a procedure yields HA films stably bound to the substrate in a polymer brush conformation [28]. To investigate the role of brush thickness and softness, we have studied three different HA surfaces made of chains of well-defined molecular weight (Hyalose, USA): two substrates obtained by incubating chains of 840 ± 60 kDa for two different times, yielding high (HA840-h) and low (HA840-l) grafting density samples, and a third one (HA58) bearing a brush made of chains of 58 ± 3 kDa. Without flow, we measure equilibrium bead heights of, respectively, $h = 405$, 285, and 110 ± 5 nm on the HA840-h, HA840-l, and HA58 layers. The gravitational force exerted by a bead sedimented on a brush reads

$$F_{\mathrm{g}} = \frac{4\pi R^3}{3} g \Delta\rho. \tag{1}$$

With $g = 9.81\ \mathrm{m\,s^{-2}}$ and a density difference of $\Delta\rho = 40\ \mathrm{kg\,m^{-3}}$ between the beads and the fluid [30], we compute $F_{\mathrm{g}} = 3.2$ pN. This corresponds to an interaction energy per unit area of $F_{\mathrm{g}}/R \simeq 2.5 \times 10^{-7}\ \mathrm{N\,m^{-1}}$ at which we anticipate the brushes to be essentially uncompressed [28]. Compared to F_{g}, van der Waals forces between the beads and the glass substrate are negligible at distances $h > 10$ nm [31], and repulsive forces of electrostatic origin are screened at the ionic strength used (Debye length < 1 nm) [32]. Therefore, as done previously with similar systems [31], we neglect surface forces and assume that quiescent beads sit at an equilibrium distance from the coverslip that reflects the unperturbed brush height H_0. From H_0, we compute (see Supplemental Material [25]) the average distance between the tethered ends of the HA chains [Fig. 1(b)], $\xi = 74 \pm 17$, 130 ± 30, and 10 ± 3 nm, respectively, for the HA840-h, HA840-l, and HA58 brushes. As a control surface, a plain gold-coated coverslip was used, passivated by a layer of bovine serum albumin to minimize nonspecific adhesive bead-surface interactions.

An example time series for h and V of a single bead traveling across the field of view is shown in Fig. 2(c).

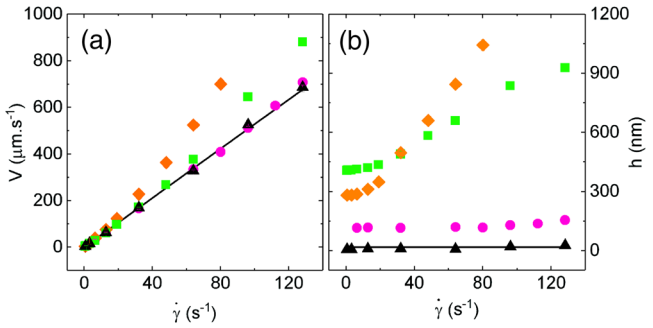

FIG. 3. (a) $V(\dot{\gamma})$ measured on control surface (solid triangle), HA840-h (solid square), HA840-l (solid diamond), and HA58 (solid circle) brushes. The solid line is the GCB prediction for nondeformable surfaces separated by 20 nm. (b) Experimentally measured $h(\dot{\gamma})$ [symbols as in panel (a)]. Solid line indicates the constant value of $z = 20$ nm used in GCB theory. Error bars accounting for standard error and uncertainty on h and V are about the size of the symbols.

Single bead data were time averaged, and measurements over 20 to 50 beads were performed under identical flow conditions to obtain the ensemble-averaged values of V and h shown, respectively, in Figs. 3(a) and 3(b) as a function of wall shear rate $\dot{\gamma} = 6Q/(WH^2)$.

On the control surface, we observe that V increases linearly with $\dot{\gamma}$, while h remains small and constant at 15 ± 10 nm over the range of $\dot{\gamma}$ explored (Fig. 3, triangles). When beads are flowing past the HA840-h brush, their velocity increases linearly with $\dot{\gamma}$ and h remains close to H_0 at shear rates below $\sim$20–30 s^{-1}. However, for $\dot{\gamma} > 30$ s^{-1}, V grows more than linearly with $\dot{\gamma}$, while h steadily increases and reaches up to 900 nm at the largest shear rate (Fig. 3, squares). Such a trend is further amplified with the HA840-l brush (Fig. 3, diamonds). With the HA58 brush, we observe that V grows quasilinearly with $\dot{\gamma}$, while h increases by only 40 nm above H_0 at the largest $\dot{\gamma}$ [Fig. 3(b) and magnified in Fig. 4(a)]. Thus, there is a lift of the beads away from the brushes, with a magnitude depending on the shear rate and the type of brush. We now discuss the possible origins of such a phenomenon.

Given the low Reynolds number in our experiments ($\mathrm{Re} \lesssim 10^{-2}$), we first compare the results from the control experiment with the theory of Goldman, Cox, and Brenner (GCB) for a rigid bead in a shear flow past a nondeformable surface [33]. For bead-surface distances $z \ll R$, GCB computed the following bead translation (V) and angular (Ω) velocities [Fig. 1(b)] [34]:

$$V = \dot{\gamma} R \frac{(1 + z/R)}{0.7625 - 0.2562 \ln(z/R)} \tag{2}$$

$$\Omega = \frac{\dot{\gamma}}{1.6167 - 0.4474 \ln(z/R)} \tag{3}$$

Using Eq. (2), we obtain excellent agreement between GCB theory, and our data on the control surface when setting $z = 20$ nm (solid lines in Fig. 3), consistent with the measured h. The results of our control experiment therefore match very well the predictions for a rigid sphere flowing in quasicontact with a rigid plane.

To address the lift from the HA surfaces, we first consider inertial forces. Even at low Re, it has been shown that an inertial lift force can act on a bead moving close to a wall in a linear shear flow [35,36]. Cherukat and McLaughlin have computed an expression for this inertial lift force, valid in the limit $z \ll R$ [36],

$$F_{\mathrm{in}} = \rho R^2 V_r^2 I(\Lambda_G, \kappa), \tag{4}$$

where $V_r = V - \dot{\gamma}(R + z)$ is the difference between the bead velocity and the fluid velocity at the location of the bead center of mass, and $I(\Lambda_G, \kappa)$ is given by

$$\begin{aligned} I = {} & [1.7669 + 0.2885\kappa - 0.9025\kappa^2 + 0.507625\kappa^3] \\ & - [3.2415/\kappa + 2.6729 + 0.8373\kappa - 0.4683\kappa^2]\Lambda_G \\ & + [1.8065 + 0.89934\kappa - 1.961\kappa^2 + 1.02161\kappa^3]\Lambda_G^2 \end{aligned} \tag{5}$$

with $\Lambda_G = \dot{\gamma}(R + z)/V_r$ and $\kappa = R/(R + z)$. Taking $V = 900$ μm s^{-1}, $\kappa \simeq 1$, and $\dot{\gamma} = 128$ s^{-1}, we estimate the maximum inertial lift force $F_{\mathrm{in}} \simeq 1.9$ pN, which is lower than F_g. Therefore, inertial effects alone cannot induce lift in the range of shear rates explored here, in agreement with our control experiment.

With electrokinetic effects [37] being negligible at the ionic strength used here (see Supplemental Material [25] and Refs. [38,39]), the only other mechanism that can lead to lift is due to EHD: in the presence of a thin and soft surface layer, elastic deformations induced by the pressure field in the lubricating fluid are predicted to give rise to a lift force (F_{EHD}) on a rigid sphere [20–22]. To test whether this accounts for our observations, we start from the expression derived by Urzay *et al.* [22] for F_{EHD},

$$F_{\mathrm{EHD}} = \frac{\eta^2 R^2 H_0 {V_s}^2}{M\delta^3} \left(\frac{48\pi}{125} + \frac{4\pi(19 + 14\omega)}{25(1 + \omega)} \frac{\delta}{R} \right), \tag{6}$$

with η the fluid dynamic viscosity, H_0 the layer thickness, M its longitudinal elastic modulus [40], δ the bead-layer distance [see Fig. 1(b)], $V_s = V - \Omega R$, and $\omega = -\Omega R/V$.

At a given shear rate, the steady-state value of δ is set by the balance of vertical forces on a bead,

$$F_{\mathrm{EHD}} + F_{\mathrm{in}} = F_g. \tag{7}$$

Equation (6) was derived for an impermeable elastic layer with a no-slip boundary condition at its surface but holds for a poroelastic layer, under conditions on M discussed below [21,41]. Moreover, a polymer brush in a shear flow is expected to be penetrated by the flow over a distance of order ξ, the interchain spacing [42–44]. We account for this by assuming the no-slip plane to lie at a distance ξ below the top of the layer [Fig. 4(a) inset]. In the spirit of previous

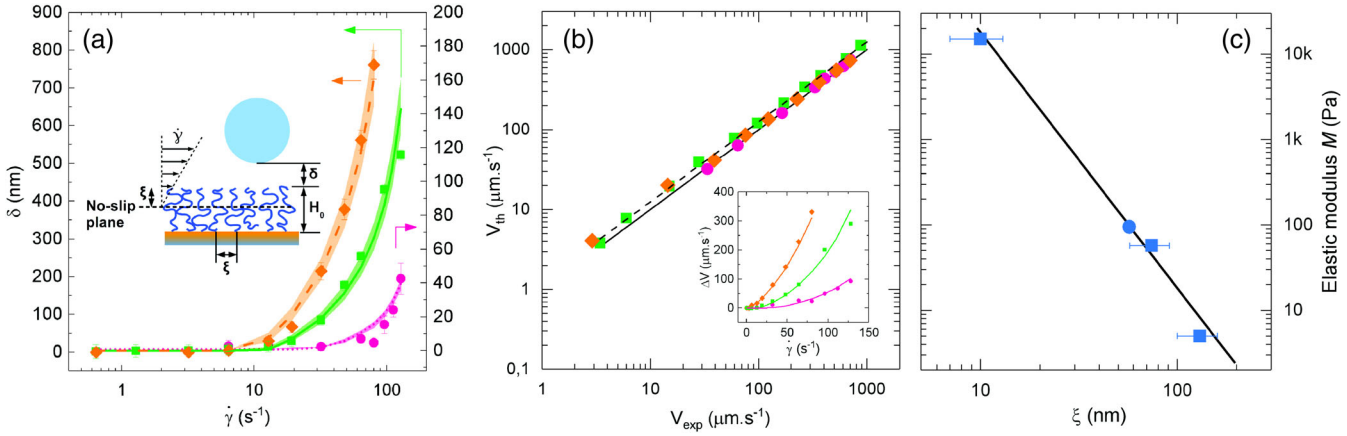

FIG. 4. (a) $h(\dot{\gamma}) - H_0$ data on HA brushes (symbols as in Fig. 3, vertical scale according to arrows) and theoretical predictions for $\delta(\dot{\gamma})$ with $M = 5$ Pa (dashed line), 57 Pa (solid line), and 15 000 Pa (dotted line). The shaded area around the theoretical curves is defined by the predictions obtained when ξ is varied from lower to upper bound for each brush. Inset: sketch showing the location of the no-slip plane at ξ below the brush surface. (b) Theoretical (V_{th}) vs experimental (V_{exp}) velocities [symbols as in panel (a)]. The solid line corresponds to $V_{\text{th}} = V_{\text{exp}}$ and the dashed line to $V_{\text{th}} = 1.2V_{\text{exp}}$. Variations of V_{th} due to changes in ξ and error bars on V_{exp} are about the symbol size. Inset: measured (symbols) and predicted (lines) deviation from linearity, $\Delta V = V(\dot{\gamma}) - S\dot{\gamma}$, with S the slope in the limit of small shear rates. (c) Best fit values (solid square), measured reference (solid circle), and predictions (solid line) for M as a function of ξ. Error bars correspond to the uncertainty on ξ.

works on hydrodynamic interactions with finite slip length [45–49], we then replace δ by $\delta + \xi$ and H_0 by $H_0 - \xi$ (the thickness of the layer not penetrated by the flow [50]) in Eq. (6). Similarly, we set $z = \delta + \xi$ in Eqs. (2)–(5), and use GCB results to compute $V_r(\dot{\gamma}, \delta)$, $V_s(\dot{\gamma}, \delta)$, and $\omega(\dot{\gamma}, \delta)$ (the above assumptions are further discussed in the Supplemental Material [25]). The theoretical values for the lift can then be determined as a function of $\dot{\gamma}$ by solving Eq. (7) for δ, knowing R, ρ, $\Delta\rho$, η, ξ, and H_0.

The resulting predictions for δ are compared with the data for $h - H_0$ in Fig. 4(a). Keeping only M as an adjustable parameter, we obtain a very good agreement between the measured and computed lift, with $M = 15\,000$, 57, and 5 Pa, respectively, for the HA58, HA840-h, and HA840-l brushes, with a marginal effect due to the uncertainty on ξ. As observed experimentally, the model predicts forces that are too low to induce lift below $\dot{\gamma} \sim$ 10–30 s^{-1} [51], while for larger shear rates the lift gradually increases, an effect that is augmented with decreasing brush modulus. Eliminating the inertial term in the force balance to account only for EHD demonstrates that inertial effects become significant for $\dot{\gamma} \geq 50$ s^{-1}, and that EHD alone accounts for about 75% of the lift observed at the highest shear rate (see Supplemental Material [25]). Besides, the velocities predicted at the corresponding $\dot{\gamma}$ and δ agree to within 20% or better with the experimental data [Fig. 4(b)], and the nonlinearity of the $V(\dot{\gamma})$ curves is quantitatively captured by the model [Fig. 4(b) inset].

Furthermore, the values of M required to reproduce the data are in agreement with previous findings on the mechanical properties of HA brushes. As for polymer gels [52], the modulus of a brush scales as $M \sim 1/\xi^3$ (see Supplemental Material [25]). From previous measurements of the mechanical response of HA brushes [28,53], we determine $M_{\text{ref}} \simeq 100$ Pa for a brush of $\xi_{\text{ref}} = 57$ nm (see Supplemental Material [25] and Refs. [54,55]). We can thus compute the expected moduli of the brushes from $M = M_{\text{ref}}/(\xi/\xi_{\text{ref}})^3$ and compare them to the above best fit values. As shown in Fig. 4(c), we obtain a good agreement between the moduli, strengthening the fact that EHD does govern the observed behaviors. Now, M_{ref} comes from quasistatic measurements and corresponds to the "drained" value of the modulus, determined under conditions where water is free to flow in the brush and does not contribute to the stiffness. Evaluating the poroelastic time of the brushes, $\tau_{\text{p}} \sim \eta H_0^2/(M\xi^2)$, and the experimental time scale $\tau_{\text{exp}} \sim \sqrt{\delta R}/V$ [21], we find that $\tau_{\text{exp}} \gg \tau_{\text{p}}$, irrespective of the brush or flow conditions. Following the argument given in [21], this confirms that the drained moduli should indeed be used in Eq. (6).

In summary, our work shows how a compliant biomimetic layer affects the near-wall motion of microparticles. Our observations are quantitatively supported by theoretical predictions based on EHD, thus providing direct evidence of soft lubrication at play at small scales. This is likely to have significant influence on the behavior of red blood cells in blood circulation. Indeed, a RBC ($R \simeq 3$ μm) flowing in plasma ($\eta \simeq 1.5$ mPa s) under a physiological shear rate $\dot{\gamma} \simeq 100$ s^{-1}, at a distance $\delta \simeq 0.5$ μm from a μm-thick glycocalyx, would experience a force $F_{\text{EHD}} \simeq$ 0.15 pN due to glycocalyx softness (which dominates over that of adjacent tissues, see Supplemental Material [25] and Ref. [56]). From a recent study of the drift velocity v_z of RBCs under shear [12], we compute $v_z = \beta\dot{\gamma}/(R + \delta)^2 \simeq 3\mu\text{m}\,\text{s}^{-1}$ at the same δ and $\dot{\gamma}$, with $\beta \simeq 0.36$ μm^3 determined

experimentally [12]. This translates into a lift force due to cell deformation $F_{\text{cell}} \sim 6\pi\eta R v_z \simeq 0.25$ pN. It thus appears that the contributions of cell and wall deformations to lubrication forces are of comparable magnitude at sub-μm distances from the wall. In conclusion, the present study underlines the important, yet often overlooked, mechanical role that the soft endothelial glycocalyx is likely to play in regulating cell-wall interactions in blood flow.

We acknowledge the "Emergence" and "AGIR" programs of Université Grenoble Alpes, the Spanish Ministry for Economy and Competiveness (project MAT2014-54867-R to R. P. R.), the European Research Council (Starting Grant No. 306435 to R. P. R.), the French Agence Nationale de la Recherche (Grant No. ANR-13-JS08-0002-01 to L. B.), and the Centre National d'Etudes Spatiales (CNES) for funding. We acknowledge the "Prestige" European program and the CNES for fellowships (H. D.). We are grateful to Liliane Coche-Guerente (Department of Molecular Chemistry, Grenoble) for assistance with surface functionalization and characterization, to Luis Yate (CIC biomaGUNE) for gold coatings, and to Gwennou Coupier (LIPhy, Grenoble) for stimulating discussions regarding the lift of RBCs.

*R.Richter@leeds.ac.uk
†lionel.bureau@univ-grenoble-alpes.fr

[1] Y. Wang, G. A. Pilkington, C. Dhong, and J. Frechette, Curr. Opin. Colloid Interface Sci. **27**, 43 (2017).
[2] D. Y. C. Chan, E. Klaseboer, and R. Manica, Soft Matter **5**, 2858 (2009).
[3] Y. Wang, C. Dhong, and J. Frechette, Phys. Rev. Lett. **115**, 248302 (2015).
[4] D. Vlassopoulos and M. Cloitre, Curr. Opin. Colloid Interface Sci. **19**, 561 (2014).
[5] T. M. Geislinger and T. Franke, Adv. Colloid Interface Sci. **208**, 161 (2014).
[6] S. Leroy, A. Steinberger, C. Cottin-Bizonne, F. Restagno, L. Léger, and É. Charlaix, Phys. Rev. Lett. **108**, 264501 (2012).
[7] R. E. Goldstein, E. Lauga, A. I. Pesci, and M. R. E. Proctor, Phys. Rev. Fluids **1**, 073201 (2016).
[8] Z. M. Jin and D. Dowson, Proc. Instn. Mech. Engrs. Part J **219**, 367 (2005).
[9] A. Kumar and M. D. Graham, Phys. Rev. Lett. **109**, 108102 (2012).
[10] H. Zhao, E. S. G. Shaqfeh, and V. Narsimhan, Phys. Fluids **24**, 011902 (2012).
[11] S. Kim, P. K. Ong, O. Yalcin, M. Intaglietta, and P. C. Johnson, Biorheology **46**, 181 (2009).
[12] X. Grandchamp, G. Coupier, A. Srivastav, C. Minetti, and T. Podgorski, Phys. Rev. Lett. **110**, 108101 (2013).
[13] M. Abkarian, C. Lartigue, and A. Viallat, Phys. Rev. Lett. **88**, 068103 (2002).
[14] P. M. Vlahovska, T. Podgorski, and C. Misbah, C.R. Phys. **10**, 775 (2009).
[15] D. A. Fedosov, B. Caswell, A. S. Popel, and G. E. Karniadakis, Microcirculation **17**, 615 (2010).
[16] P. Olla, Phys. Rev. Lett. **82**, 453 (1999).
[17] T. W. Secomb, R. Hsu, and A. R. Pries, Am. J. Physiol. **274**, H1016 (1998).
[18] E. R. Damiano, B. R. Duling, K. Ley, and T. C. Skalak, J. Fluid Mech. **314**, 163 (1996).
[19] E. R. Damiano, D. S. Long, F. H. El-Khatib, and T. M. Stace, J. Fluid Mech. **500**, 75 (2004).
[20] J. Beaucourt, T. Biben, and C. Misbah, Europhys. Lett. **67**, 676 (2004).
[21] J. M. Skotheim and L. Mahadevan, Phys. Fluids **17**, 092101 (2005).
[22] J. Urzay, S. G. Llewellyn Smith, and B. J. Glover, Phys. Fluids **19**, 103106 (2007).
[23] B. Rallabandi, B. Saintyves, T. Jules, T. Salez, C. Schönecker, L. Mahadevan, and H. A. Stone, Phys. Rev. Fluids **2**, 074102 (2017).
[24] B. Saintyves, T. Jules, T. Salez, and L. Mahadevan, Proc. Natl. Acad. Sci. U.S.A. **113**, 5847 (2016).
[25] See Supplemental Material at http://link.aps.org/supplemental/10.1103/PhysRevLett.120.198001 for details concerning RICM setup and analysis, brush characterization, magnitude of electroviscous lift, modeling assumptions, brush mechanics and substrate effect.
[26] J. Raedler and E. Sackmann, Langmuir **8**, 848 (1992).
[27] J. Schilling, K. Sengupta, S. Goennenwein, A. R. Bausch, and E. Sackmann, Phys. Rev. E **69**, 021901 (2004).
[28] S. Attili, O. V. Borisov, and R. P. Richter, Biomacromolecules **13**, 1466 (2012).
[29] E. Migliorini, D. Thakar, R. Sadir, T. Pleiner, F. Baleux, H. Lortat-Jacob, L. Coche-Guerente, and R. P. Richter, Biomaterials **35**, 8903 (2014).
[30] M. Orlishausen, L. Butzhammer, D. Schlotbohm, D. Zapf, and W. Köhler, Soft Matter **13**, 7053 (2017).
[31] A. Albersdörfer and E. Sackmann, Eur. Phys. J. B **10**, 663 (1999).
[32] J. N. Israelachvili, *Intermolecular and Surface Forces*, 3rd ed. (Academic Press, Amsterdam, 2011).
[33] A. J. Goldman, R. G. Cox, and H. Brenner, Chem. Eng. Sci. **22**, 653 (1967).
[34] Numerical coefficients slightly differ from the original formula by GCB. We have fitted the values tabulated in Ref. [33] and found that the present set of coefficients yields a better agreement than those provided in the original publication.
[35] G. P. Krishnan and D. T. Leighton, Jr., Phys. Fluids **7**, 2538 (1995).
[36] P. Cherukat and J. B. Mclaughlin, J. Fluid Mech. **263**, 1 (1994).
[37] S. G. Bike, L. Lazarro, and D. C. Prieve, J. Colloid Interface Sci. **175**, 411 (1995).
[38] S. M. Tabatabaei, T. G. M. van de Ven, and A. D. Rey, J. Colloid Interface Sci. **301**, 291 (2006).
[39] J. M. Nielsen, A. W. Adamson, and J. W. Cobble, J. Am. Chem. Soc. **74**, 446 (1952).
[40] $M = E(1-\nu)/[(1+\nu)(1-2\nu)]$, with E the Young modulus and ν the Poisson ratio.
[41] A. Gopinath and L. Mahadevan, Proc. R. Soc. B **467**, 1665 (2011).

[42] J. L. Harden, O. V. Borisov, and M. E. Cates, Macromolecules **30**, 1179 (1997).
[43] T. Lee, S. C. Hendy, and C. Neto, Macromolecules **45**, 6241 (2012).
[44] M. Deng, X. Li, H. Liang, B. Caswell, and G. E. Karniadakis, J. Fluid Mech. **711**, 192 (2012).
[45] A. A. Potanin and W. B. Russel, Phys. Rev. E **52**, 730 (1995).
[46] J. Lee and A. J. C. Ladd, Phys. Fluids **14**, 1631 (2002).
[47] J. Baudry, E. Charlaix, A. Tonck, and D. Mazuyer, Langmuir **17**, 5232 (2001).
[48] C. Cottin-Bizonne, S. Jurine, J. Baudry, J. Crassous, F. Restagno, and E. Charlaix, Eur. Phys. J. E **9**, 47 (2002).
[49] E. Charrault, T. Lee, C. D. Easton, and C. Neto, Soft Matter **12**, 1906 (2016).
[50] M. A. C. Stuart, F. H. W. H. Waajen, T. Cosgrove, B. Vincent, and T. L. Crowley, Macromolecules **17**, 1825 (1984).
[51] From the force balance and Eq. (6), the shear rate $\dot{\gamma}_c$ above which lift sets in is such that $V_s(\dot{\gamma}_c, \xi) \sim \sqrt{F_g M \xi^3/(\eta^2 R^2 (H_0 - \xi))}$.
[52] M. Rubinstein and R. H. Colby, *Polymer Physics* (Oxford University Press, Oxford, England, 2003), p. 259.
[53] S. Attili and R. P. Richter, Soft Matter **9**, 10473 (2013).
[54] E. Gacoin, C. Fretigny, A. Chateauminois, A. Perriot, and E. Barthel, Tribol. Lett. **21**, 245 (2006).
[55] K. L. Johnson, *Contact Mechanics* (Cambridge University Press, Cambridge, England 1985), pp. 104–105.
[56] S. Leroy and E. Charlaix, J. Fluid Mech. **674**, 389 (2011).